UNIVERSITY OF BIRMINGHAM
University of Birmingham
Research at Birmingham

# Post-fabrication functionalization of 4D printed polycarbonate photopolymer scaffolds

Brooks, Scott L; Arno, Maria Chiara; Dove, Andrew; Weems, Andrew

*DOI:*
10.1021/acsapm.2c00648

*License:*
None: All rights reserved

*Document Version*
Peer reviewed version

*Citation for published version (Harvard):*
Brooks, SL, Arno, MC, Dove, A & Weems, A 2022, 'Post-fabrication functionalization of 4D printed polycarbonate photopolymer scaffolds', *ACS Applied Polymer Materials*, vol. 4, no. 8, pp. 5670–5679. https://doi.org/10.1021/acsapm.2c00648

Link to publication on Research at Birmingham portal

**Publisher Rights Statement:**
This document is the Accepted Manuscript version of a Published Work that appeared in final form in ACS Applied Polymer Materials, copyright © American Chemical Society after peer review and technical editing by the publisher. To access the final edited and published work see: https://doi.org/10.1021/acsapm.2c00648

**General rights**
Unless a licence is specified above, all rights (including copyright and moral rights) in this document are retained by the authors and/or the copyright holders. The express permission of the copyright holder must be obtained for any use of this material other than for purposes permitted by law.

•Users may freely distribute the URL that is used to identify this publication.
•Users may download and/or print one copy of the publication from the University of Birmingham research portal for the purpose of private study or non-commercial research.
•User may use extracts from the document in line with the concept of 'fair dealing' under the Copyright, Designs and Patents Act 1988 (?)
•Users may not further distribute the material nor use it for the purposes of commercial gain.

Where a licence is displayed above, please note the terms and conditions of the licence govern your use of this document.

When citing, please reference the published version.

**Take down policy**
While the University of Birmingham exercises care and attention in making items available there are rare occasions when an item has been uploaded in error or has been deemed to be commercially or otherwise sensitive.

If you believe that this is the case for this document, please contact UBIRA@lists.bham.ac.uk providing details and we will remove access to the work immediately and investigate.

Download date: 17. Apr. 2024

This document is confidential and is proprietary to the American Chemical Society and its authors. Do not copy or disclose without written permission. If you have received this item in error, notify the sender and delete all copies.

# Post-fabrication functionalization of 4D printed polycarbonate photopolymer scaffolds

| | |
|---|---|
| Journal: | *ACS Applied Polymer Materials* |
| Manuscript ID | ap-2022-006485.R1 |
| Manuscript Type: | Article |
| Date Submitted by the Author: | n/a |
| Complete List of Authors: | Brooks, Scott; Ohio University, Mechanical Engineering<br>Arno, Maria; University of Birmingham, Chemistry<br>Dove, Andrew; University of Birmingham, School of Chemistry<br>Weems, Andrew; Ohio University, Mechanical Engineering |
| | |

SCHOLARONE™
Manuscripts

# Post-fabrication functionalization of 4D printed polycarbonate photopolymer scaffolds

Scott Brooks[1], MC Arno[2], AP Dove[2*], AC Weems[1-3*]

[1]Department of Mechanical Engineering, , Russ College of Engineering, Ohio University, Athens, OH, 45701, USA

[2]School of Chemistry, University of Birmingham, Edgbaston, Birmingham, B15 2TT, UK

[3]Biomedical Engineering Program, Translational Biosciences Program, Russ College of Engineering, Ohio University, Athens, OH, 45701, USA

Corresponding email address: weemsac@ohio.edu

*KEYWORDS: 3D Printing, Shape Memory Polymer, Photopolymer, Thiol-ene Click Chemistry, Surface Functionalization*

**Abstract**

Photopolymerization has been widely used to create crosslinked photoset materials that have found wide applicability, including in 3D printing. Among the many chemistries available for these processes, thiol-ene "click" chemistry provides a rapid and efficient route to produce such materials but also leaves residual alkene groups which may be further exploited for post-polymerization functionalization. In the case of aliphatic polycarbonates, these residual functional groups are demonstrated to be suitable for controlling the thermo-solvation response by modifying hydrophobicity, enhancing radio-density and biostability through incorporation of an alkylthiol chains (*i.e.* hexadecanethiol) or halogenation using molecular iodine, and reducing biofouling using thiol-terminated poly(ethylene glycol). To further enhance the potential for post-fabrication modification, we further demonstrate the concept with off-stoichiometry stereolithographic 3D printing (OSS3DP), where we can selectively leave more than 30% additional alkenes on the scaffold surface for post-polymerization functionalization in a process that could have clinical utility across a range of medical devices and therapeutics.

**Introduction**

3D printing (3DP) has gained significant interest in recent years due to both its unique manufacturing capabilities and its promise for tissue engineering, biomanufacturing, medical devices, and many other fields.[1-5] One of the major limitations that prevents the wide-spread implementation of 3DP is however, the lack of available materials and functionalities in the printed parts, including both advanced properties such as shape memory as well as the possibilities of modifying the printed surface after fabrication.

A large number of studies have examined photopolymer biomaterial systems, focusing primarily on acrylate- and epoxide-containing materials, as well as a host of crosslinking reactions such as acrylates and allyl-groups.[6-10] Ignoring the limitations of these materials with regards to possible toxicity or degradation behavior, 3D printing photopolymers universally suffer from three disadvantages: uncontrolled cellular adhesion, limited stimuli-responsiveness or advanced properties, and low density thereby limiting visibility under x-rays.[11-13] It may be expected that the continued exploitation of the same acrylates and epoxide-materials, which have continuously been studied or proposed for biomaterials, will reinforce these limitations, and therefore new materials should be considered to address these challenges.

In efforts to address these limitations, recent work with thiol-ene, thiol-yne, reversible deactivation radical polymerization, and free radical crosslinking using in-chain alkenes has been attempted with varying degrees of success.[1, 11, 14, 15] A recent study by Roppolo *et al.* focused on a thiol-yne type method of digital light processing (DLP) printing, where excess functional groups would allow for post-polymerization modification.[16] This method, while successful, was limited by the achievable resolution of the scaffold, but successfully demonstrated that high concentrations of either residual alkene or thiol functional groups could be incorporated into the structure.[16] Wilson *et al.* utilized an end-functionalized poly(propylene fumarate) (PPF) system for copper-catalyzed "click" reactions post-polymerization, where the initial crosslinking occurred *via* free-radical crosslinking at the in-chain alkenes with involvement of the diethylfumarate reactive diluents.[17] This technique was further employed to incorporate fluorescent dyes on the surface of the printed films, demonstrating sufficient residual functional group concentrations to perform significant post-printing modifications, opening avenues into inclusions of other materials such as osteogenic growth factor or bone morphogenic protein.[18] Kleinfehn *et al.* again expanded this concept by including physical additives (bioglass) that could be modified using catechol in the same PPF materials.[19] Bioderived β-myrcene and poly(β-myrcene) have further been demonstrated to be photocrosslinkable in thiol-ene resins, where residual alkenes may be used to tailor material hydrophobicity using alkyl thiols in simple post-fabrication irradiative processes.[20]

Taking inspiration from these works, we have developed a methodology for post-polymerization functionalization leveraging thiol-ene "click" photochemistry of previously described aliphatic polycarbonates, utilizing residual surface alkenes or using off-stoichiometric stereolithographic 3D printing (OSS3DP) to provide sites for covalent bonds to form on the scaffold surfaces in an effort to alter a wide array of behaviors, including hydrophobicity, cellular adhesion, degradation rates, and optical density (for x-ray imaging). Through modifications of hydrophobicity using small hydrocarbons, we are able to change the rate of water influx into the polycarbonate bulk as a method of altering thermo-solvation shape memory effects. This method is also used to decrease cellular adhesion on the surface of printed scaffolds compared with unmodified scaffolds. Halogenation of the polycarbonates was additionally used to increase optical density of the materials and modify degradation rates, while maintaining mechanical behavior of the scaffolds.

## Results and Discussion

Organobase-catalyzed ring opening polymerization (ROP) of cyclic aliphatic carbonates was selected for its ease-of-use, scalability, and synthetic reproducibility as demonstrated previously.[21] The ROP of aliphatic cyclic carbonates has previously allowed us to produce homopolymer poly(trimethylolpropane allyl carbonate) (TMPAC), an aliphatic polycarbonate containing allyl (TMPAC) with $M_n \sim 1.5$ kDa and $Đ_M \sim 1.1$-1.4.[21] $^1$H NMR and FT-IR spectroscopy (Figure 1A and *Supplemental Material Figure S1)* were used to confirm crosslinking of the films, matching previously reported results.[21] Resins were formulated by mixing oligomeric polycarbonates (homopolymers and random copolymers) with reactive diluents previously described and the 4-arm thiol crosslinker pentaerythritol tetrakis(mercaptopropanoic acid) (PETMP) (Scheme 1A), after which the photoinitiator Irgacure 819 and photoinhibitor, capsanthin, were added at 0.5 wt%, respectively, and was used to produce porous scaffolds similar to those previously described (Scheme 1B). The molar concentration of the polycarbonates was varied to produce different off-stoichiometric ratios, as desired, while the amounts of the diluents and PETMP were held constant.

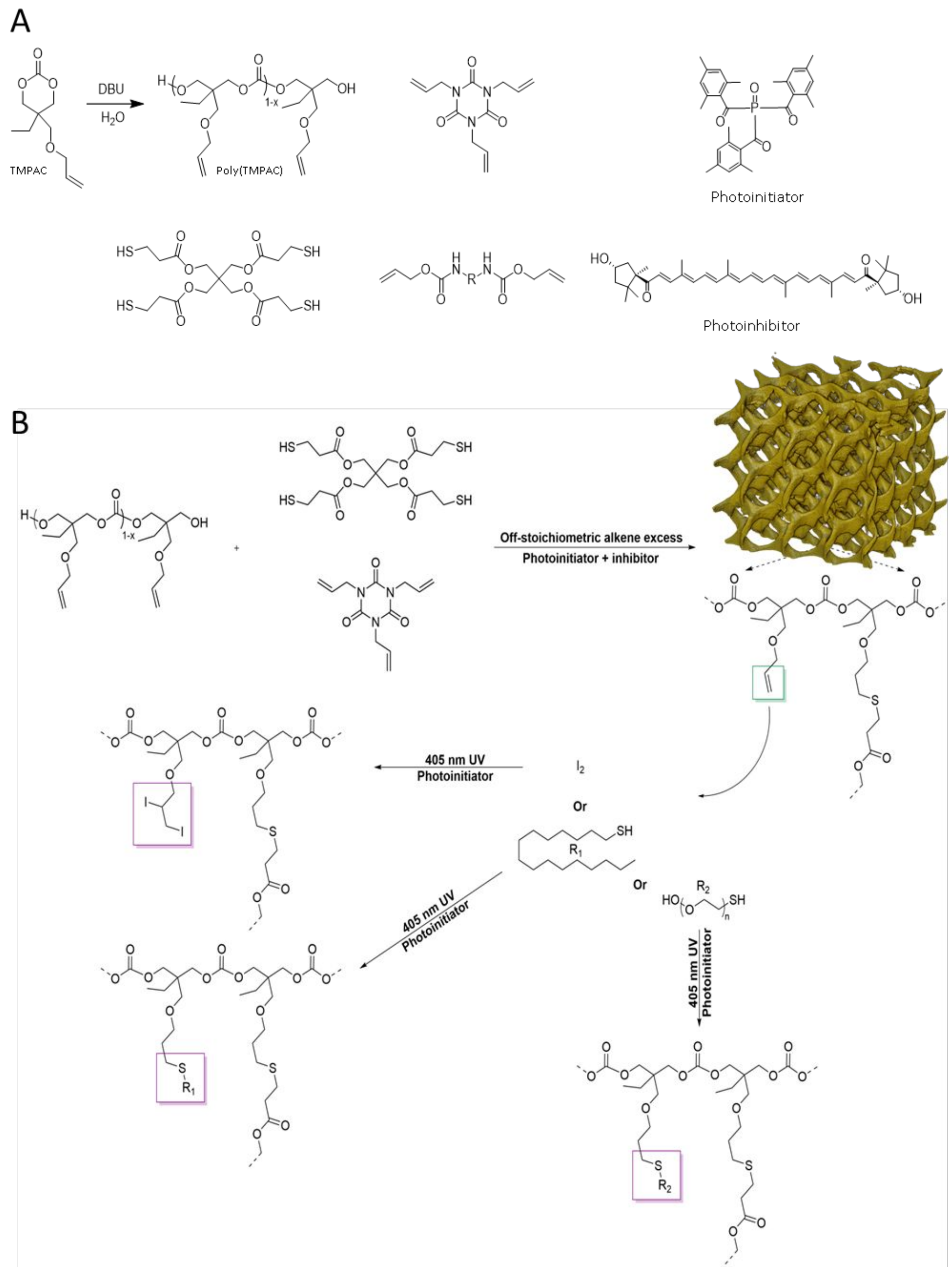


**Scheme 1.** Schematic representation of polyTMPAC polycarbonate produced from cyclic TMPAC monomer using organo-base catalyzed reactions, along with the resin components including reactive diluent representative species, PETMP, photoinitiator and photoinhibitor species (A). A representative microCT image of the 3D printed porous scaffold is displayed along with idealized carbonate linkages including crosslinked sites and residual alkenes, which are used to post-polymerization functionalize the monolith after fabrication (B).

*Off-Stoichiometry 3D Printing*

3D printing of the resins was optimized to $\lambda = 405$ nm light as previously described, allowing for the production of a variety of different printed products including porous tissue scaffolds with reproducible features below 250 µm.[21] The crosslinked material was analyzed by NMR spectroscopy (Figure 1A, samples irradiated by a light source of $\lambda = 405$ nm and power of 10 $mW \cdot cm^{-2}$, samples irradiated at ambient conditions, 20 °C, resins dissolved in $CDCl_3$ prior to irradiation) and FT-IR spectroscopy, with residual allyl groups centered at $\delta = 5.83$ (m) and 5.19 (dd) ppm, most likely due to the limited diffusion possible in the crosslinked, solidified material during the gelation process. During the initial 15 s of irradiation, which is qualitatively at least 1.5 times the amount of time necessary to produce thin, porous tissue scaffolds, there were approximately 30% residual allyl groups (and corresponding thiol groups) as determined by $^1$H NMR spectroscopy (Figure 1B). Importantly, the residual alkenes and thiols are present in a mechanically stable crosslinked solid, or, the less-than-idealized crosslinking does not compromise the integrity of the final printed part or the rate at which crosslinking occurs. Ultimately, this means that the solidified resins will have residual functional groups after irradiation but prior to thermal treatment, which in photopolymerizations will allow for layer integration but may also be used for post-fabrication functionalization.

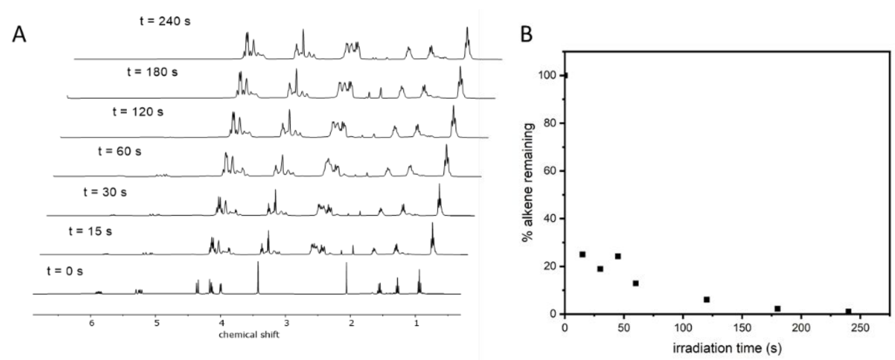


**Figure 1.** (A) $^1$H NMR spectra of irradiated poly(TMPAC) and PETMP resins (1 wt% Irg 819), with resins irradiated at $\lambda = 370$ nm to 410 nm at 10 $mW \cdot cm^{-2}$ at ambient conditions, 20 °C, 500 MHz NMR in $CDCl_3$, tested at 298 K, and (B) corresponding quantified alkene concentrations determined at discrete timepoints displaying residual alkenes after more than 2 min of irradiation.

Identification of the residual alkenes in the 3D printing resin photosets inspired us to optimize this feature to maximize functional concentration on the material surface for post-fabrication functionalization reactions. Further increasing the concentration of residual allyl groups after solidification, was achieved by using an excess of poly(TMPAC) (up to 30% excess allyl), and off-stoichiometry photopolymerization gelation kinetics were examined using photorheology. The storage modulus (*G*') (Figure 2A) and loss factor (tan $\delta$) of the resin were studied. Their behaviors displayed distinct increases in *G*' as a function of irradiation time and a peak loss factor associated with a phase transition from the liquid resin to the gelled solid polymer in similar conditions to those that the resin would experience in the 3D printer during layer solidification.

Photopolymer resins containing up to 15% excess poly(TMPAC) (allyl groups) displayed equivalent gelation times and all yielded solid thermosets upon photoirradiation. Gelation times increased from *ca* 2 s (stoichiometrically balanced photopolymer resins through 15% excess alkene) to 4 s for resins with 25% allyl excess groups, and nearly doubled again to 7 s at 30% excess alkene, as determined by the loss factor peak value (Figure 2B). Importantly, for 20% excess and less, the storage modulus behavior is nearly identical, and the changes in time to plateauing moduli or phase transition are subtle. While Flory-Stockmayer theory may be used to theoretically determine that poly(TMPAC) (DP ~ 10) can form a thermoset network, this gelation does not equate to solid polymer formation. Furthermore, photopolymer resins possessing 30% excess of poly(TMPAC) display a reduced green mechanical stability, indicated by the nearly an order of magnitude reduction in storage modulus after gelation compared with the 20% excess materials. This indicates that greater off-stoichiometric ratios beyond 20-25% excess would likely result in the mechanical failure of the part during the SLA process.[22, 23] It should be noted, however, in the 20% excess resins more than 50% alkenes could remain after photocuring during the 3D printing process without sacrificing feature resolution down to 250 μm.

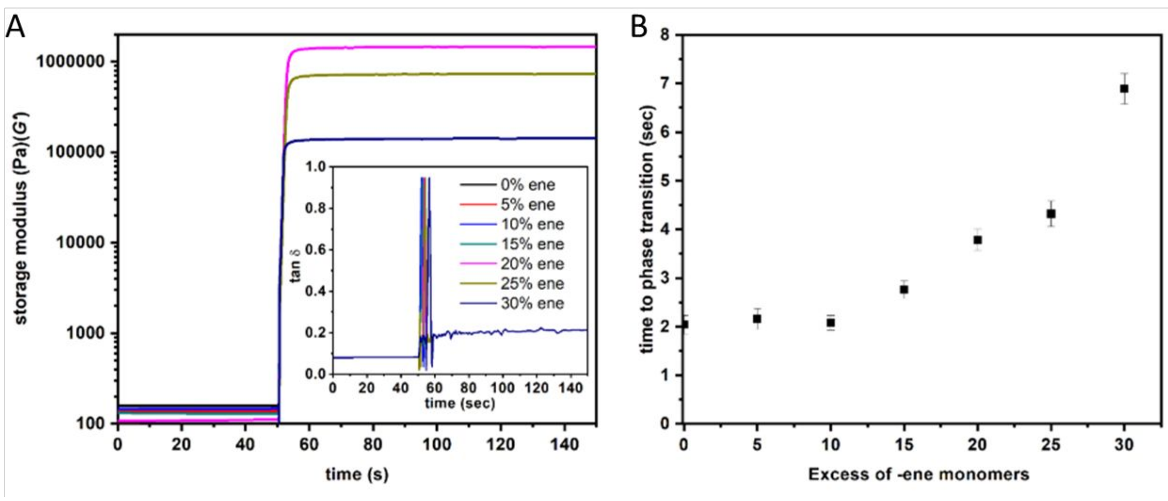


**Figure 2**. Representative photorheology gelation kinetics of storage moduli with the loss factor (tan δ) (inset) (A) and the corresponding average gelation time (B) of poly(TMPAC) and PETMP resins (1 wt% Irg 819), with resins irradiated at $\lambda$ = 370 nm to 520 nm at 10 mW·cm$^{-2}$ at ambient conditions, 20 °C, n = 3.

*Surface Hydrophobicity and Thermo-Solvation Induced Shape Memory Response*

4D materials, 3D printed structures which possess the ability to respond to stimuli after fabrication, are promising candidates for an array of technologies, such as minimally invasive medical therapeutics for materials which display shape memory behaviors.[24-26] Understanding how to tune this 4D behavior is important towards controlling the shape change in medical device applications, particularly with regards to the amount of time that a clinician has to work before shape recovery occurs.[26] This working time occurs as a consequence of thermo-solvation-induced property migration, often due to plasticization of hydrogen-bonded groups which in turn results in a decrease of the and the observed glass transition temperature ($T_g$). Uncontrolled strain recovery behaviors, particularly in porous media, would reduce the so-called "working time" with the material and ultimately limit the clinical utility unless the infiltration of plasticizing agent was addressed without altering the bulk composition.

The interaction of the solvent, water or phosphate buffered saline in medical applications, with the polymer surface drives the initial 4D behavior in the clinic. The rate of solvent infiltration will control the rate chain relaxation. This allows for the design of the clinical working time. With OSS3DP, the residual alkenes may be leveraged for functionalization with alkylthiol such as hexadecanethiol. For poly(TMPAC) photosets, the materials display contact angles ranging from 55° to 75° with an excess of allyl groups ranging from 0% excess to 30% excess (Figure 3A). Importantly, off stoichiometric photosets are statistically different from 0% excess poly(TMPAC). Treatment of the surfaces with hexadecanethiol resulted in statistically different material surfaces, however all the surfaces displayed similar contact angles of ~80° with similar advancing contact angle relaxations (Figure 3B).

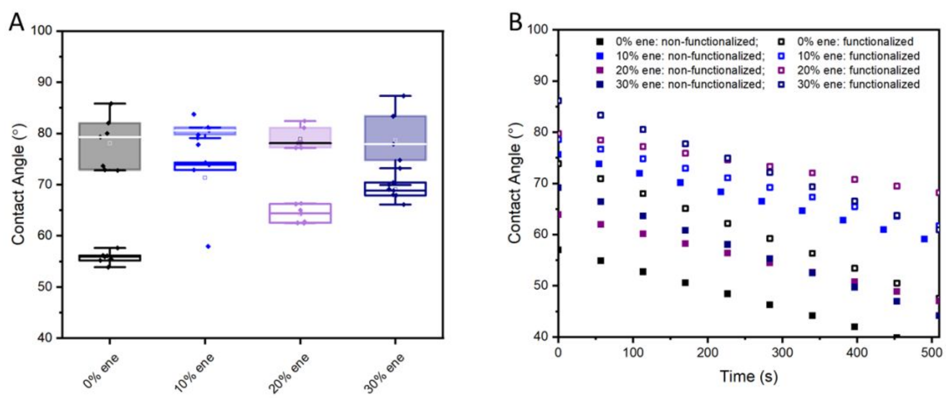


**Figure 3**. Water contact angle before and after thiol-ene surface treatment with hexadecanethiol for different off-stoichiometry poly(TMPAC) photosets (A) and representative advancing contact angle of photoset films before and after treatment with hexadecanethiol (B). (n = 7)

The 4D printing aspect of these polycarbonate materials was previously noted for the low recovery stresses and high recovery strains they are capable of displaying (self-fitting behavior in hydrogels, for instance), as well as the tunability as a function of polycarbonate and urethane crosslinker composition.[27] Unfunctionalized, crosslinked films display rapid shape recovery when plasticized (wet $T_g$ of 34.5 ± 1.4˚C) as determined using immersion DMA (the dry $T_g$ of these materials were previously characterized as 43.9 ± 2.4 °C).[27] When the films were irradiated ($\lambda$ = 370 nm to 520 nm at 10 mW·cm$^{-2}$ at ambient conditions, 20 °C) in a solution of hexadecanethiol, acetone, and photoinitiator for 1 h, this behavior was found to change, despite the material displaying an equivalent $T_g$, indicating that post-fabrication functionalization occurs primarily at the material surface. For example, at 37 ˚C (in PBS) films which would ordinarily undergo rapid shape recovery from a bent configuration to a straightened form within moments were found instead to only slightly recover (*Supplemental Materials Figure S2*). Over a 5 min period, the unmodified control film would display a more rapid strain recovery, while the surface-modified film displayed a reduced rate of recovery, qualitatively.

Mechanical examination of the films revealed the untreated films would go through phase change from a more glassy material to a more rubbery one over the course of 10 minutes.[28] The peak tan $\delta$ value, typically assumed to be the point at which such viscoelastic regime change occurs, was found at approximately 240 s, corresponding to the shape recovery behavior found in the bulk.[28] However, in the modified materials, no peak tan $\delta$ value was found. Instead, over a 15 minute period the material continued to become more rubbery (decreasing storage modulus) but did not undergo a phase change indicative of shape recovery onset, which matches the reduced rate of shape recovery found in the deformed films.

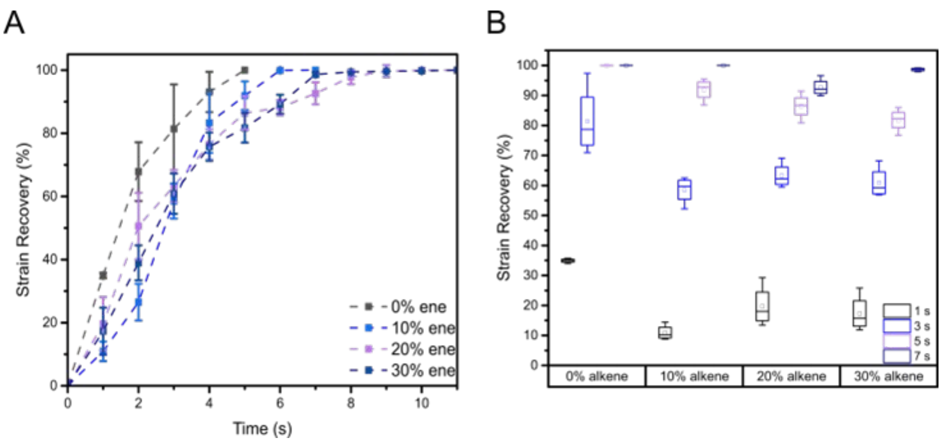


**Figure 4.** (A) Strain recovery kinetics of poly(TMPAC) films immersed in 37 °C $H_2O$ comparing post-polymerization functionalization with hexadecanethiol on various off-stoichiometric films and (B) corresponding strain recoveries at discrete time points. (n = 4)

*Scaffold Halogenation*

Residual alkenes also offered an opportunity to address the x-ray density limitation found in most polymeric medical devices and scaffolds using a very simple approach: halogenation of the residual alkenes using iodine.[29-31] When considering minimally invasive devices intended to reduce patient risk by guiding the device delivery with clinical imaging, as opposed to open surgery, the need for visualization of the material using conventional clinical imaging techniques, specifically x-ray, becomes apparent.[32] While previous attempts to incorporate x-ray imaging have utilized compositing or small molecule additives (covalently crosslinked or physically added), these methods ultimately result in the migration of scaffold properties, rather than simply changing suface chemistry without affecting bulk behavior.[28] These risks, in addition to obvious difficulties in incorporating additional moieties into 3DP resins and the desire to retain the bulk material properties of the original material, also make this method less ideal. Surface modification to selectively incorporate chemical x-ray contrast agents, therefore, is the most appealing candidate, and previous examinations of alkenes have indicated that halogenation of alkenes may be achieved using simple methods, such as heating in the presence of chlorine or iodine with acetone.[29-31, 33]

Halogenation of residual alkenes in the printed scaffolds, using a modified method where the scaffolds are exposed to molecular iodine in acetone for 12 h at 50 °C, was found to enhanced the optical density of the scaffolds as determined using micro-CT imaging (*Supplemental Materials Figure S3*).[31] The scaffolds displayed 1.5× x-ray contrast after this treatment as measured by pixel-density from microCT imaging compared with the original porous scaffolds. Importantly, this post-polymerization treatment could be incorporated into the typical cleaning protocol required for extractions and washings, allowing for the removal of both leachable compounds as well as residual iodine or other attached species. Attempts at functionalizing the cylic monomer and oligomer were also successful, but reduced the workability of the photopolymer resin, leading us to pursue post-polymerization as an easier and more efficient process.

Iodination of the polycarbonate scaffolds also provide alternative methods for tuning degradability in both static and dynamic degradation analysis (Figure 5). Dynamic degradation analysis (0.1 N dynamic load, 1 Hz oscillatory tensile load of bar films at 5 M NaOH at 37 ˚C) demonstrated a rapid loss of mechanical stability for the unmodified polycarbonate, revealing a rapid plasticization behavior associated with thermo-solvent relaxation followed by a loss of mechanical integrity over the next 40 h period. This behavior seems to be dominated by two regimes: the first most likely corresponding to the surface erosion found at less accelerated conditions and *in vivo*, and the second more rapid loss as a result of microcracking prior to material failure. By contrast, the halogenated samples display substantially greater mechanical stability, both regarding the decreased relaxation behavior found due to plasticization as well as the increased time to loss of the storage modulus maxima. Importantly, static gravimetric analysis (Figure 5A insert) supported this observed behavior, with iodinated scaffolds presenting increased biostability in these aggressive hydrolytic conditions.

The loss factor of the materials was in line with the mechanical and gravimetric analyses (Figure 5B). The control polycarbonates display a rapid relaxation within the first hours of immersion in solution, often associated with plasticization. The loss factor plateaus for a time, after which it begins to increase prior to failure, indicating substantial changes in the materials behavior likely associated with cracking. This behavior was found to be reproducible across polycarbonate compositions, with the final storage moduli amplitudes and times to failure varying with the same behaviors. By comparison, the iodinated polycarbonates show a slight antiplasticization behavior at the initial immersion time, noted by the increasing loss factor. Hydrolysis eventually overcomes this regime, as noted by the approximately 130 h constant decrease in loss factor, leading to eventual material failure following surface erosion. Uniaxial mechanical compression on the DMA also indicated that despite these biostability differences, the mechanical response of the bulk scaffold was only slightly enhanced (*Supplemental Material Figure S4*).

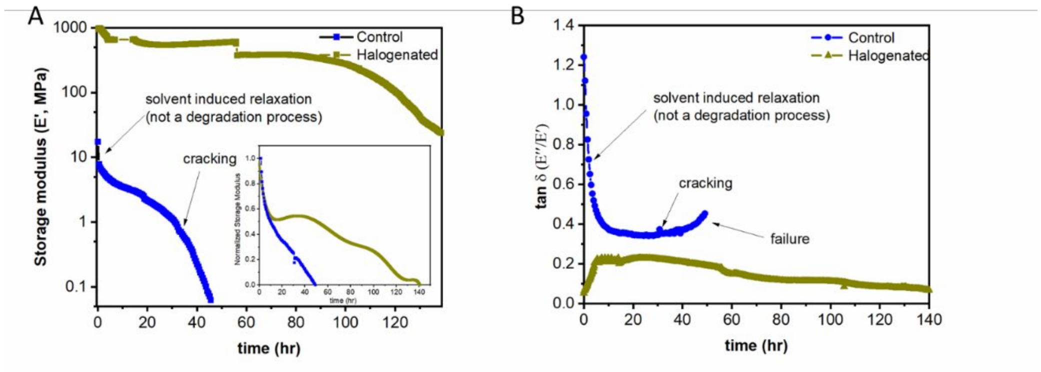


**Figure 5**. Dynamic degradation representative curves comparing the poly(TMPAC) and the iodinated sample immersed in 5 M NaOH at 37 °C with regards to storage moduli over time (A) along with inset gravimetric degradation and loss factor (B).

*Cellular Response to Scaffold Surfaces*

Finally, cytocompatibility of the polymers and surface treatments was examined using MC3T3 murine pre-osteoblasts through a PrestoBlue proliferation assay over one- and two-week time periods. Compared to glass and PLLA, standard biomaterial controls, as well as unfunctionalized poly(TMPAC) scaffold and a porous poly(TMPAC) as a further control material, the post-fabrication functionalized materials displayed similar cytocompatibilities (*Supplemental Materials Figure S5*). The surface modifications resulted in no significant differences in cell viability over the examined time periods, with the polycarbonates maintaining the high cytocompatibility demonstrated previously with the control materials.[27]

With cytocompatibility established, surfaces functionalized with poly(ethylene glycol) (PEG) (to reduce cellular adhesion and biofouling for implants) and other biologically relevant surfaces such as amine and aldehyde functional groups were examined.[34-36] PEGylation, by the nature of the highly flexible PEG chains, reduces protein adsorption and thereby can reduce cellular adhesion, which may be advantageous for applications such as cardiovascular stents, where the continued exposure of the stent surface may lead to thrombogenesis at the stent and unwanted downstream embolization.[37] Monothiol-terminated $PEG_{50}$ was functionalized to the porous polycarbonate scaffolds in a solution of PEG:DI $H_2O$:acetone:photoinitiator solution (1:2:0.02: 0.005 weight, irradiated as described earlier) and compared to control medium and untreated scaffolds.[27] The test articles were then immersed for 24 h in cell media followed by seeding cells on the scaffold surface. As expected, the treated scaffold displayed reduced fluorescence compared with the untreated scaffolds (Figure 6). Repeating the surface functionalization using acrolein or cysteamine, which produced aldehyde- and primary amine-functionalized surfaces, respectively, did statistically alter cytocompatibility as determined from comparison of Day 1 and Day 7 cellular viabilities (compared using a Student's T-Test, two tailed) (*Supplemental Material Figures S6 and S7)* and adds further avenues for enhancing tissue adhesion or controlling cellular differentiation *in vitro* in future work.[38, 39] This is compared with the untreated surfaces, which display no difference in cellular viability over the same time period.

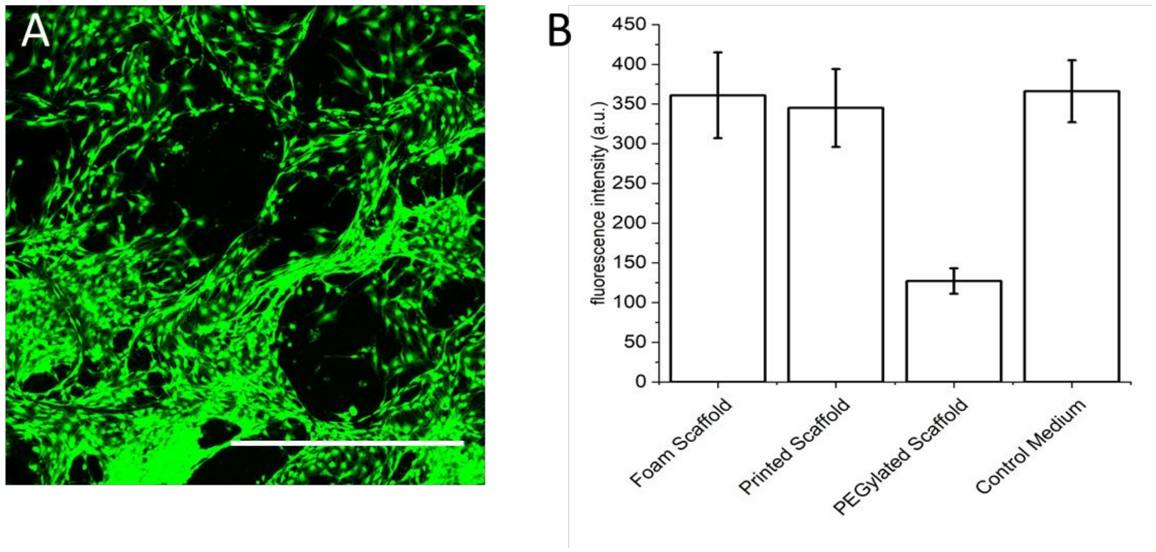


**Figure 6**. Representative fluorescence microscopy image of 3D printed poly(TMPAC) porous tissue scaffold seeded with MC3T3 pre-osteoblasts after 7 days incubation (A) and the effect of the increased hydrophobicity, achieved through incorporation of $PEG_{50}$ onto the polycarbonate scaffold through modification of the residual alkene functional groups, resulting in decreased cellular adhesion as demonstrated through fluorescence intensity comparisons after absorption of proteins from cell culture media onto material surfaces (B). (scale bar = 500 μm)

This type of behavior could find benefit in a variety of biological applications, such as reducing biofouling or reducing cellular infiltration rates for certain procedures. Importantly, this modification does not alter the bulk biocompatibility, which has been demonstrated for the control polycarbonate formulations, as PEGylated surfaces will still hydrolytically degrade and leave behind surfaces to which proteins will be better able to adsorb and ultimately allow for delayed cellular adhesion and infiltration into the scaffold.[27]

## Conclusions

Using porous polycarbonate scaffolds, we demonstrate the use of OSS3DP as a platform material technology to meet these needs. These scaffolds, which may possess up to 30% excess thiol or allyl groups for post-polymerization functionalization, hold substantial promise for a variety of healthcare technologies. We further demonstrate the ability to modify 3D printed scaffold behavior without requiring off-stoichiometric imbalances in our starting photopolymer resins, leveraging residual alkenes to modify the thermo-solvation-induced plasticized shape recovery behaviors. The residual surface alkenes may also be halogenated to enhance radio-density using iodination of the printed scaffolds, which further provides an additional handle to alter the biostability of the materials without sacrificing bulk properties. Finally, we demonstrate that these alkenes may also be leveraged to alter the biological response to the material, most notably to reduce biofouling of the scaffold surfaces. Importantly, these surface modifications do not alter the cytocompatibility of the poly(TMPAC), indicating that this may be a clinically-valid technique to incorporate additional material functionalities with established biomaterials.

## Supporting Information

$^1$H NMR and FT-IR spectra along with additional photorheology, dynamic mechanical analysis, shape memory imaging, X-ray imaging and analysis, and cell viability analysis are provided in the supporting information

## Acknowledgements

ACW would like to thank the Whitaker Foundation, as well as the Marie Sklodowska-Curie Grant (#793247), and Ohio University (start-up funding). Prof. Matthew Gibson is thanked for giving access to his cell lab facilities. The University of Warwick Advanced BioImaging Research Technology Platform, BBSRC ALERT14 award BB/ M01228X/1 are thanked for confocal fluorescence microscopy analysis.

## Conflicts of Interest

ACW and APD are named inventors on a patent relating to this work which is being commercialized by a spin-out company, 4D Biomaterials Ltd of which they are founders and shareholders. APD is also the Chief Scientific Officer for 4D Biomaterials.

## Methods and Materials

*Instrumentation:* All starting reagents were commercially available (purchased from Sigma-Aldrich unless otherwise stated) and used without further purification. Solvents were of ACS grade or higher. NMR spectra (400 MHz for $^1$H and 125 MHz for $^{13}$C) were recorded on a Bruker 400 spectrometer and processed using MestReNova v9.0.1 (Mestrelab Research, S.L., Santiago de Compostela, Spain). Chemical shifts were referenced to residual solvent peaks at $\delta$ = 7.26 ppm ($^1$H) and $\delta$ = 77.16 ppm ($^{13}$C) for $CDCl_3$ and $\delta$ = 2.50 for ($^1$H) and $\delta$ = 39.52 ppm ($^{13}$C) for $d_6$-DMSO. Size exclusion chromatography (SEC) was performed using an Agilent 1260 Infinity II Multi-Detector GPC/SEC System fitted with RI and ultraviolet (UV) detectors ($\lambda$ = 309 nm) and PLGel 3 μm (50 × 7.5 mm) guard column and two PLGel 5 μm (300 × 7.5 mm) mixed-C columns with $CHCl_3$ with 5 mM triethylamine as the eluent (flow rate 1 mL/min, 50 °C). A 12-point calibration based on poly(methyl methacrylate) standards (PMMA, Easivial PM, Agilent) was applied for determination of molecular weights and dispersity ($Đ_M$). Fourier transform infrared spectroscopy (FT-IR) was performed in attenuated total reflectance (ATR) mode on a Bruker infrared spectrometer (Bruker, Billerica, MA) using 50 scans, background subtraction, atmospheric correction, and a spectral resolution of 2 cm$^{-1}$. An Anton Paar rheometer (Anton Paar USA Inc, Ashland, VA, USA) fitted with a detachable photoillumination system with two parallel plates (10 mm disposable aluminum hollow shaft plate, Anton Paar) was used for rheology studies.

Dynamic mechanical analysis was performed using a Mettler-Toledo TT-DMA system (Mettler-Toledo AG, Schwerzenbach, Switzerland) fitted with an equilibrating water bath and water circulator, and samples analyzed using Mettler-Toledo STARe v.10.00 software. 3D printing scaffolds and templates were processed using Solidworks (Dassault Systemes, Vélizy-Villacoublay, France) and cicro-computed tomography analysis was performed using a Skyscan 1172 MicroCT (e2v technologies plc, Chelmsford, UK) at an isotropic pixel size of 7-13 µm, a camera exposure time of 500 ms, a rotation step of 0.4°, frame averaging of 5 and medium filtering with a flat field correction. Image reconstruction was performed using a NRecon 1.6.2 (SkyScan, e2v technologies plc, Chelmsford, UK).

*Synthesis of aliphatic polycarbonate:* Ring opening polymerization of the cyclic monomers was used to obtain alcohol-terminated oligomers, synthetic steps of which are described elsewhere.[27] In general, $CHCl_3$ and cyclic monomer(s) were added to a round-bottomed flask followed by 1,8-diazabicyclo[5.4.0]undec-7-ene (DBU). For polyTMPAC, TMPAC (100 g, 500.0 mmol) was dissolved in 100 mL $CHCl_3$. DBU (1.44 g, 9.5 mmol) and water (150 µL, 8.3 mmol) were added in a single aliquot. The resulting solution was stirred for 24 h at 20 °C, after which the DBU was quenched with the addition of Amberlyst A15 $H^+$ acidic resin, precipitated into ice cold hexanes, and then filtered through a silica plug in ethyl acetate. The solution was concentrated *in vacuo* to yield a viscous, colorless liquid (96.2 g, 96%). $^1$H NMR ($CDCl_3$, 400 MHz,): $\delta$ = 0.87 (t, $^3J_{H\text{-}H}$ = 7.6 Hz, 3H), 1.48 (d, $^3J_{H\text{-}H}$ = 9.4 Hz, 2H), 3.32 (s, 2H), 3.92 (dd, $^3J_{H\text{-}H}$ = 5.4 Hz $^3J_{H\text{-}H}$ = 1.8 Hz, 2H), 4.10 (m, 4H), 5.26 (m, 2H), 5.80 (m, 1H). $^{13}$C NMR ($CDCl_3$, 125 MHz;): $\delta$ = 7.45, 22.58, 41.87, 67.78, 69.46, 72.27, 116.73, 134.67, 155.15. SEC ($CHCl_3$) $M_n$: 2.1 kDa, $Đ_M$ = 1.29

*Formulation of poly(TMPAC) resins*. polyTMPAC and urethane-based reactive diluent were added to a vial, along with the 4 arm tetrathiol (pentaerythritol tetrakis(3-mercaptopropionate) (PETMP)). As an example, the polyTMPAC resin consisted of isophorone di(allyl urethane) reactive diluent (13.78 g, 40.7 mmol), polyTMPAC (15.28 g, 7.6 mmol), 1,3,5-triallyl-1,3,5-triazine-2,4,6(1H,3H,5H)-trione as a second reactive diluent species (14.65 g, 58.7 mmol), PETMP (24.41 g, 53.2 mmol), and of propylene carbonate as an unreactive diluent (16.54 g, 162.1 mmol) mixed together for 8 h at ambient conditions. To this was added Irgacure 819 (photoinitiator, 0.82 g, 1 wt%), and paprika extract (photoinhibitor, 0.50 g, 0.75 wt%) in a dark room with little ambient light, followed by 1 h of stirring. After homogenization of the resin, the resin was placed in a brown glass container and stored at room temperature in the dark. To produce off-stoichiometry resins, the concentration of the PETMP was reduced or increased by the desired percentage (up to 30% excess of alkene), leaving an excess of alkene or thiol groups.

*3D Printing*: Scaffolds based upon previously reported geometries were printed from resins using varied conditions dependent upon composition.[27, 40] Resins were added in 100 mL quantities to the resin tray, allowing for complete and even coverage of the optical window and the surface of the printing plate. Porous scaffolds were printed by applying the photomask (MiiCraft 50×, BURMS, Jena, Germany) and corresponding irradiation to the 50 µm thick slice at 20 s intervals, using $\lambda$ = 405 nm light. Base plates were burned in from polyTMPAC resin at 75 s, with four layers to secure the print; per slice time was varied by photoinhibitor concentration, however approximately 20 s was typically sufficient without overcuring. Post-printing, samples were cut from the plate and immersed in acetone for approximately 1 h to remove residual resin ink. Other printed monoliths were printed with slight variations in printing conditions. After the cleaning with acetone, printed samples were allowed to dry overnight at ambient conditions.

*Post-fabrication Modifications:* A solution of the functionalizing molecule and acetone was made with the greatest concentration possible. The acetone (10 wt% for hexadecanethiol, cysteamine, acrolein, and iodine) was necessary for all reactions. Photoinitiator (Irgacure 819, 2 wt%) was added to all but the halogenation solutions. DI $H_2O$ and acetone was used for the thiol-terminated $PEG_{50}$ solution (1:2:0.02: 0.005 weight, PEG:$H_2O$:acetone:). For photopolymerization functionalization, the polycarbonate films were first photocured using the aforementioned 3D printing conditions, at which time the films were immersed in the solution and irradiated for 3 h (370 nm to 520 nm at 10 $mW \cdot cm^{-2}$ at ambient conditions, 20 °C), after which the films were removed and allowed to dry in ambient conditions for 12 h, followed by 120 °C oven cure for 24 h. Iodination was performed on solid polycarbonate films and scaffolds following the protocol established by Pavlinac *et al*, modified to use 10% acetone during the treatment to allow for better solubility and surface coverage of the scaffolds.[30]

*Photorheology.* Crosslinking kinetics of resin samples were examined as a function of gelation time by measuring the dampening or phase ratio (tan $\delta$), storage moduli, loss moduli, complex viscosity, and film thickness during photorheology. Resin samples were sheared between two parallel plates, one made of glass and transparent, at 1 Hz for 50 sec without irradiation. After this time, the resins were irradiated with $\lambda$ = 430-520 nm light and measurements were taken every 0.2 s over the course of 2 min. The inflection points of the moduli plots, and the peak tan $\delta$ values, were used to determine the time to gelation of the resin. Sample shrinkage was measured by measuring the distance between the plates at the same sampling rate as the other metrics.

*Dynamic Mechanical Analysis:* Rectangular dynamic mechanical analysis (DMA; Mettler-Toledo TT-DMA system (Mettler-Toledo AG, Schwerzenbach, Switzerland)) samples were prepared *via* 3D printing sample bars (2.0 cm × 0.5 cm × 0.2 cm). Samples were analyzed in tension mode using autotension mode, with a frequency of 1 Hz, a preload force of 1 N, and a static force of 0.1 N. The measurements were analyzed using Mettler-Toledo STARe v.10.00 software. Three samples were used in each analysis.

Relaxation kinetics studies of the printed scaffolds were conducted using submersion DMA at 37°C in phosphate buffered saline (PBS) solution. Scaffolds (1 $cm^3$) were placed in compression and deformed 10 μm, 1 Hz with a preload of 0.1 N at ambient conditions for approximately 60 s. At this time, the scaffold was then immersed in the PBS solution and held isothermally as the same load was applied for 60 min. Storage moduli and tan δ values were recorded as a function of time to determine the behavior of the polymer during initial submersion/introduction to biologically-mimicking conditions.

*Contact angle testing:* Glass slides were spin coated with 0%, 10%, 20%, and 30% excess-ene off-stoichiometric films and photocured, one with excess hexadecane thiol and one without, for 1 h and subsequently thermally cured for 24 h at 120 °C. 12 μL of deionized $H_2O$ was deposited onto the slides and the initial contact angle recorded and contact angle relaxation measured over the span of 10 minutes with images being recorded every 10 s. The contact angle was measured using Ossila Contact Angle v 3.0.7.0 software on an Osilla Contact Angle goiniometer (Sheffield, UK).

*Shape memory testing:* Polymer films (15 mm in length, 3 mm thick, 5 mm wide) were heated to 60 °C and bent 180°. After deformation, films were held strained until they had cooled to ambient conditions, at which time the film is immersed in 37°C PBS, the strain is released and the angle between the film arms was measured.

After post-fabrication functionalization of the 0%, 10%, 20%, and 30% excess-ene polymer films, they were bent 180° in ambient conditions and strained in 10 °C DI $H_20$ for 60 s at which time the films were immersed in 20 °C DI $H_20$ and the resultant strain recovery was measured until full relaxation had occurred while measuring the displacement between both ends of the polymer film against relaxation time.

*Degradation Analysis*: Porous scaffolds and non-porous scaffolds were immersed in degradation solution, following previously established protocols for static degradation analysis for determining gravimetric changes over time in 0.1 and 5 M NaOH.[41] For dynamic degradation studies, films were tested using DMA and 5 M NaOH solution at 37 °C, loaded with a 0.1 N pre-load and 10 Hz oscillation using a modified plasticization study design reported previously.[28] Samples were tested until failure, with the phase ratio and the storage moduli recorded over the course of the study.

*Cytocompatibility and Cellular Analysis:* Cytocompatibility was performed in 2D and 3D as previously described, using MC3T3 pre-osteoblasts purchased from ATCC UK and cultured in Alpha Minimum Essential Medium with ribonucleosides, deoxyribonucleosides, 2 mM L-glutamine and 1 mM sodium pyruvate, but without ascorbic acid, supplemented with 10% FBS and 1% pen/strep, at 37 °C and 5% $CO_2$. For 2D experiments, films were spin coated on glass slides, using 5 wt% solutions of photocrosslinked resin in $CHCl_3$.[21] Slides were then sterilised with 70% ethanol and inserted in 12 well plates. Cells were seeded on top of the films at a concentration of 2,000 cells/cm$^2$. PrestoBlue viability assay (Thermofisher) was performed at day 1, 3, 7, and 14 of incubation, following manufacturer's protocol and fluorescence was recorded using a BioTek microplate reader (λ ex. = 560 nm, λ em. = 610 nm). For 3D experiments, scaffolds were first sterilized in 70% ethanol and incubated for 24 h in cell culture medium. The media was then removed and MC3T3 cells were seeded on the top surface of the scaffolds (100,000 in 20 µL of medium) which were then incubated at 37 °C and 5% $CO_2$. Media (2 mL) was then added after 3 h to completely submerge the scaffolds which were incubated again for 1, 3, and 7 days. At the selected time point, the scaffolds were washed with PBS and incubated with a live/dead assay kit (Invitrogen), which provides staining of live cells with calcein (λ ex. = 495 nm, λ em. = 515 nm) and dead cells with ethidium homodimer (λ ex. = 528 nm λ em. = 617 nm). Samples were then imaged using a Zeiss LSM 880 confocal microscope equipped with Airyscan, using a 5× air objective and 488 nm and 594 nm lasers. Z-stacks with an average thickness of 200 µm were collected from different zones of each sample, and the images were processed using ImageJ software.

*Protein adsorption analysis:* The FluoroProfile Protein Quantification Kit (Sigma Aldrich) was used to quantify protein adsorption to the printed scaffolds. Bovine Serum Albumin (BSA, 2 mg) was dissolved in 1 mL of PBS. 100 µL of this stock solution were diluted with 900 µL of quantitation buffer (as supplied in the FluoroProfil kit) to reach a final concentration of 200 µg/mL.

A further dilution with PBS to 12 ng/mL was performed to get the final protein concentration for the quantification assay. From this solution, 100 μL was placed in a 96 well plate together with 100 μL of sample (foam scaffold, printed scaffold, PEGylated scaffold, and cell medium). Samples were incubated for 30 min. and the fluorescence was recorded using a BioTek microplate reader (λ ex. = 530 nm, λ em. = 645 nm).

## References

(1) Ligon, S. C.; Liska, R.; Stampfl, J.; Gurr, M.; Mulhaupt, R. Polymers for 3D Printing and Customized Additive Manufacturing. *Chem Rev* **2017**, *117* (15), 10212-10290. DOI: 10.1021/acs.chemrev.7b00074.
(2) Chia, H. N.; Wu, B. M. Recent advances in 3D printing of biomaterials. *J Biol Eng* **2015**, *9*, 4. DOI: 10.1186/s13036-015-0001-4.
(3) Dodziuk, H. Applications of 3D printing in healthcare. *Kardiochir Torakochirurgia Pol* **2016**, *13* (3), 283-293. DOI: 10.5114/kitp.2016.62625.
(4) Gopinathan, J.; Noh, I. Recent trends in bioinks for 3D printing. *Biomater. Res.* **2018**, *6* (22), 11. DOI: 10.1186/s40824-018-0122-1.
(5) Zhang, S.; Wang, H. Current Progress in 3D Bioprinting of Tissue Analogs. *SLAS Technology* **2019**, *24* (1), 70-78, Review. DOI: 10.1177/2472630318799971 Scopus.
(6) Deng, Y.; Li, J.; He, Z.; Hong, J.; Bao, J. Urethane acrylate-based photosensitive resin for three-dimensional printing of stereolithographic elastomer. *J. Appl. Polym. Sci.* **2020**, *137* (42), 49294. DOI: 10.1002/app.49294.
(7) Dhulst, E. A.; Heath, W. H.; Torkelson, J. M. Hybrid Thiol-Acrylate-Epoxy Polymer Networks: Comparison of One-Pot Synthesis with Sequential Reactions and Shape Memory Properties. *Polymer* **2016**, *96*, 198-204. DOI: 10.1016/j.polymer.2016.04.032.
(8) Ding, R.; Du, Y.; Goncalves, R. B.; Francis, L. F.; Reineke, T. M. Sustainable near UV-curable acrylates based on natural phenolics for stereolithography 3D printing. *Polym. Chem.* **2019**, *10* (9), 1067-1077. DOI: 10.1039/c8py01652f.
(9) Fairbanks, B. D.; Schwartz, M. P.; Bowman, C. N.; Anseth, K. S. Photoinitiated polymerization of PEG-diacrylate with lithium phenyl-2,4,6-trimethylbenzoylphosphinate: polymerization rate and cytocompatibility. *Biomaterials* **2009**, *30* (35), 6702-6707. DOI: 10.1016/j.biomaterials.2009.08.055.
(10) Gojzewski, H.; Guo, Z.; Grzelachowska, W.; Ridwan, M. G.; Hempenius, M. A.; Grijpma, D. W.; Vancso, G. J. Layer-by-Layer Printing of Photopolymers in 3D: How Weak is the Interface? *ACS Appl. Mater. Interfaces* **2020**, *12* (7), 8908-8914. DOI: 10.1021/acsami.9b22272.
(11) Weems, A. C.; Perez-Madrigal, M. M.; Arno, M. C.; Dove, A. P. 3D Printing for the Clinic: Examining Contemporary Polymeric Biomaterials and Their Clinical Utility. *Biomacromolecules* **2020**, *21* (3), 1037-1059. DOI: 10.1021/acs.biomac.9b01539.
(12) Autian, J. Structure-Toxicity Relationships of Acrylic Monomers. *Environ. Health Perspect.* **1975**, *11*, 141-158.
(13) Black, B. J.; Ecker, M.; Stiller, A.; Rihani, R.; Danda, V. R.; Reed, I.; Voit, W. E.; Pancrazio, J. J. In vitro compatibility testing of thiol-ene/acrylate-based shape memory polymers for use in implantable neural interfaces. *J Biomed Mater Res A* **2018**, *106* (11), 2891-2898. DOI: 10.1002/jbm.a.36478.
(14) Bagheri, A.; Fellows, C. M.; Boyer, C. Reversible Deactivation Radical Polymerization: From Polymer Network Synthesis to 3D Printing. *Adv Sci (Weinh)* **2021**, *8* (5), 2003701. DOI: 10.1002/advs.202003701 From NLM PubMed-not-MEDLINE.
(15) SL Brooks, E. C., OM King, AC Weems. Stereochemistry and stoichiometry in aliphatic polyester photopolymers for 3D printing tailored biomaterial scaffolds. *Polym. Chem.* **2022**, *13* (14), 2048-2056.
(16) Roppolo, I.; Frascella, F.; Gastaldi, M.; Castellino, M.; Ciubini, B.; Barolo, C.; Scaltrito, L.; Nicosia, C.; Zanetti, M.; Chiappone, A. Thiol–yne chemistry for 3D printing: exploiting an off-stoichiometric route for

selective functionalization of 3D objects. *Polym. Chem.* **2019**, *10* (44), 5950-5958. DOI: 10.1039/c9py00962k.
(17) Wilson, J. A.; Luong, D.; Kleinfehn, A. P.; Sallam, S.; Wesdemiotis, C.; Becker, M. L. Magnesium Catalyzed Polymerization of End Functionalized Poly(propylene maleate) and Poly(propylene fumarate) for 3D Printing of Bioactive Scaffolds. *J. Am. Chem. Soc.* **2018**, *140* (1), 277-284. DOI: 10.1021/jacs.7b09978.
(18) Li, S.; Xu, Y.; Yu, J.; Becker, M. L. Enhanced osteogenic activity of poly(ester urea) scaffolds using facile post-3D printing peptide functionalization strategies. *Biomaterials* **2017**, *141*, 176-187. DOI: 10.1016/j.biomaterials.2017.06.038.
(19) Kleinfehn, A. P.; Lammel Lindemann, J. A.; Razvi, A.; Philip, P.; Richardson, K.; Nettleton, K.; Becker, M. L.; Dean, D. Modulating Bioglass Concentration in 3D Printed Poly(propylene fumarate) Scaffolds for Post-Printing Functionalization with Bioactive Functional Groups. *Biomacromolecules* **2019**, *20* (12), 4345-4352. DOI: 10.1021/acs.biomac.9b00941.
(20) Weems, A. C.; Delle Chiaie, K. R.; Yee, R.; Dove, A. P. Selective Reactivity of Myrcene for Vat Photopolymerization 3D Printing and Post-Fabrication Surface Modification. *Biomacromolecules* **2019**, *21* (1), 163-170. DOI: 10.1021/acs.biomac.9b01125.
(21) Weems, A. C.; Arno, M. C.; Yu, W.; Huckstepp, R. T.; Dove, A. P. 4D polycarbonates via stereolithography as scaffolds for soft tissue repair. *Nature communications* **2021**, *12* (1), 1-14.
(22) Ware, H. O. T.; Farsheed, A. C.; Akar, B.; Duan, C.; Chen, X.; Ameer, G.; Sun, C. High-speed on-demand 3D printed bioresorbable vascular scaffolds. *Materials Today Chemistry* **2018**, *7*, 25-34. DOI: 10.1016/j.mtchem.2017.10.002.
(23) Yang, C.-H.; Jeyaprakash, N.; Chan, C.-K. Inhomogeneous mechanical properties in additively manufactured parts characterized by nondestructive laser ultrasound technique. *NDT & E International* **2020**, *116*, 102340. DOI: 10.1016/j.ndteint.2020.102340.
(24) Gladman, A. S.; Matsumoto, E. A.; Nuzzo, R. G.; Mahadevan, L.; Lewis, J. A. Biomimetic 4D printing. *Nat Mater* **2016**, *15* (4), 413-418. DOI: 10.1038/nmat4544.
(25) Hendrikson, W. J.; Rouwkema, J.; Clementi, F.; van Blitterswijk, C. A.; Fare, S.; Moroni, L. Towards 4D printed scaffolds for tissue engineering: exploiting 3D shape memory polymers to deliver time-controlled stimulus on cultured cells. *Biofabrication* **2017**, *9* (3), 031001. DOI: 10.1088/1758-5090/aa8114.
(26) Javaid, M.; Haleem, A. 4D printing applications in medical field: A brief review. *Clinical Epidemiology and Global Health* **2019**, *7* (3), 317-321. DOI: 10.1016/j.cegh.2018.09.007.
(27) Weems, A. C.; Arno, M. C. A.; Huckstepp, R. T. R.; Dove, A. P. 4D Polycarbonates via Stereolithography as Scaffolds for Soft Tissue Repair *Nat. Commun.* **2021**, *12* (1), 1-14.
(28) Weems, A. C. R., J.E.; Wacker, K.T.; Gustafson, T.P.; Keller, B.; Wooley, K.L.; Maitland, D.J. Examination of Radio-oopacity Enhancing Additives in Shape Memory Polyurethane Foams. *J. Appl. Polym. Sci.* **2015**, *132* (23), 10.1002/APP.42054.
(29) Carbone, A. S., M; Uhrich, KE. Iodinated Salicylate-Based Poly(anhydride-esters) as Radiopaque Biomaterials. *Biomacromolecules* **2008**, *8*, 1604-1612.
(30) Pavlinac, J.; Zupan, M.; Stavber, S. Solvent-free iodination of organic molecules using the I(2)/urea-H(2)O(2) reagent system. *Org Biomol Chem* **2007**, *5* (4), 699-707. DOI: 10.1039/b614819k.
(31) Yemets, S. V.; Shubina, T. E.; Krasutsky, P. A. Electrophilic monoiodination of terminal alkenes. *Org Biomol Chem* **2013**, *11* (17), 2891-2897. DOI: 10.1039/c3ob27348b.
(32) Anderson, P. J.; Yong, R.; Surman, T. L.; Rajion, Z. A.; Ranjitkar, S. Application of three-dimensional computed tomography in craniofacial clinical practice and research. *Aust. Dent. J.* **2014**, *59 Suppl 1*, 174-185. DOI: 10.1111/adj.12154.
(33) Beloglazkina, E. K. T., V.S.; Zyk, N.V.; Grishin, Y.K. An Unusual Way of the Reaction of PI3 with Norbornene and Norbornadiene. *Russ. Chem. Bull.* **1997**, *46* (3), 496-500.

(34) Antony, G. J. M.; Jarali, C. S.; Aruna, S. T.; Raja, S. Tailored poly(ethylene) glycol dimethacrylate based shape memory polymer for orthopedic applications. *J Mech Behav Biomed Mater* **2017**, *65*, 857-865. DOI: 10.1016/j.jmbbm.2016.10.011.
(35) Aoki, D.; Ajiro, H. Design of Polyurethane Composed of Only Hard Main Chain with Oligo(ethylene glycol) Units as Side Chain Simultaneously Achieved High Biocompatible and Mechanical Properties. *Macromolecules* **2017**, *50* (17), 6529-6538. DOI: 10.1021/acs.macromol.7b00629.
(36) Schuster, F.; Hirth, T.; Weber, A. Reactive inkjet printing of polyethylene glycol and isocyanate based inks to create porous polyurethane structures. *J. Appl. Polym. Sci.* **2019**, *136* (3), 46977. DOI: 10.1002/app.46977.
(37) Deglau, T. E.; Maul, T. M.; Villanueva, F. S.; Wagner, W. R. In vivo PEG modification of vascular surfaces for targeted delivery. *J Vasc Surg* **2012**, *55* (4), 1087-1095. DOI: 10.1016/j.jvs.2011.09.081.
(38) Cao, B.; Peng, Y.; Liu, X.; Ding, J. Effects of Functional Groups of Materials on Nonspecific Adhesion and Chondrogenic Induction of Mesenchymal Stem Cells on Free and Micropatterned Surfaces. *ACS Appl. Mater. Interfaces* **2017**, *9* (28), 23574-23585. DOI: 10.1021/acsami.7b08339.
(39) Olivia, N. C., M; Beckerman, M; Seliktar, S; Hayward, A; Stanley, J; Parry, NM; Edelman, ER; Artzi, N. Regulation of dendrimer/dextran material performance by altered tissue microenvironment in inflammation and neoplasia. *Sci Transl Med* **2015**, *7* (272), 272ra211.
(40) Merckle, D.; Constant, E.; Cartwright, Z.; Weems, A. Ring Opening Copolymerization (ROCOP) of 4D Printed Shape Memory Polyester Photopolymers using Digital Light Processing. *Macromolecules* **2021**, *54* (6), 2681-2690.
(41) Weems, A. C. W., KT; Carrow, JK; Boyle, AJ; Maitland, DJ. Shape Memory Polyurethanes with Oxidation-Induced Degradation_ In Vivo and In Vitro Correlations for Endovascular Material Applications. *Acta Biomater.* **2017**, *59*, 33-44.